NUMERICAL AND EXPERIMENTAL VALIDATION OF UNITIZED BEAM MODEL

Danzi, Francesco* **, Cestino, Enrico*** **, Frulla, Giacomo*** **, Gibert, James M.****
* **Politecnico di Torino, **Ray W. Herrick Lab, Purdue University**

Keywords: *Beam, Homogenization, Optimization, Stiffened structure, Variable Stiffness*

Abstract

This paper presents the numerical and experimental validation of a variable stiffness box beam model made by an arrangement of stiffened and unstiffened panels. The derivation of the equivalent properties of curvilinear stiffened plates is briefly summarized. The validity of the equivalent continuum plate model is assessed. The governing equations of the variable stiffness box-beam are presented. Once the model is established, the stiffeners' path to attain a desired static performance is sought. The optimal configuration is determined by a topology optimization problem where the design variables become the orientation of the curved stiffeners at prescribed points. Several analytical examples along with one experiment are presented to show the validity of the model presented herein.

1 Introduction

Aircraft's contribution to global CO2 emission has come under scrutiny since the early 2000s. In response to rising concentrations of green house gas, the 36-State ICAO Council has adopted a new aircraft CO2 emissions standard, which aims to reduce the impact of aviation's greenhouse gas emissions on the global climate (Annex 16, Volume III). Environmental Responsible Aviation (ERA) of NASA's Fundamental Aeronautic Programme provides guidelines and emission targets for future generation aircraft. Gains in energy efficiency by modifying the wing through structural weight reduction and to have higher as-

pect ratios (HAR). The resulting slender, lighter and highly flexible structures are prone to exhibit aeroelastic instabilities [1, 2, 3]. Additionally anisotropic materials can play a crucial role enhancing aircraft performance by maintaining rigidity and allowing deformation coupling with no additional penalties on weight. To this end, aeroelastic tailoring is a fundamental tool, as reported in the review paper of Jutte and Stanford [4]. The first record of aeroelastic tailoring is dated back in 1949 by Munk[5], where wooden propeller blade were oriented to create desirable deformation couplings when operated. In the late 1960s, there was a thrust in aeroelastic tailoring research, which has continued steadily through to today. In Weisshaar *et al* [6], it has been shown that certain aeroelastic tailoring methods can modify the wing's primary stiffness direction, changing the wing's bending and torsional stiffness as well as the degree of coupling between the two. Those methods are known as global (uniform) aeroelastic tailoring. On the other end, when separate sections of the wing are tailored differently from one another, aeroelastic tailoring is applied in a more *"local"* manner over the wing. These methods are used especially when composite materials are concerned [7, 8, 9, 10, 11].

Potential enabling technologies for passive aeroelastic tailoring are: Functionally Graded Materials (FGM) [12], Variable Angle Tow (VAT) [13] and curvilinear stiffeners [14]. Previous research efforts have proposed models with different level of computational complexity to deal with aero-structural design of HAR wing.

While overlooked in most research effort, the idealized models have a prominent effect on the final aircraft; outcomes they provide may influence considerably the entire life-cycle costs [15, 16]. These models in fact, represent the physics of the problem, using a minimum number of degrees of freedom and design variables, rendering the models to have low fidelity that can qualitatively predict the aircraft's behavior.

In this work, we present a numerical and experimental validation of a unitized box beam model subjected to different load conditions. The box beam considered has a rectangular cross section. The upper and lower panels are stiffened by means of steering stiffeners; the shear webs are C spars. The local orientation of the stiffeners is presumed to vary linearly according to equation proposed by Wu[17] and Wang [18, 19]. The stiffened panels are in the concentric or symmetric configuration. The present paper extend the current body of research in that it introduces curved stiffeners, previous investigations were restricted to consider straight but oriented stiffeners [20, 21]. The aim of the paper is to identify the stiffeners' path that maximize the bending-torsion coupling while ensuring a tip deflection lower than a prescribed limit. Different load configurations are considered.

The reminder of the paper is organized as follow: section 2 summarizes the derivation of the mathematical model adopted herein. Particularly, section 2.1 presents the equivalent plate stiffness of steering stiffened panels; the equivalent plate model is validated via Finite Element Analysis (FEA) comparing buckling loads and frequencies of simply supported plates obtained with the equivalent model against those obtained with a detailed model. Section 2.2, provides the equations used to calculate the cross sectional stiffnesses of the beam. Section 3 summarizes the main features of the optimization algorithm implemented and presents the mathematical formulation of the optimization problem. In section 4 the results obtained with the numerical procedure are discussed; a comparison with an experiment is also presented. Finally, in section 5, there are concluding remarks.
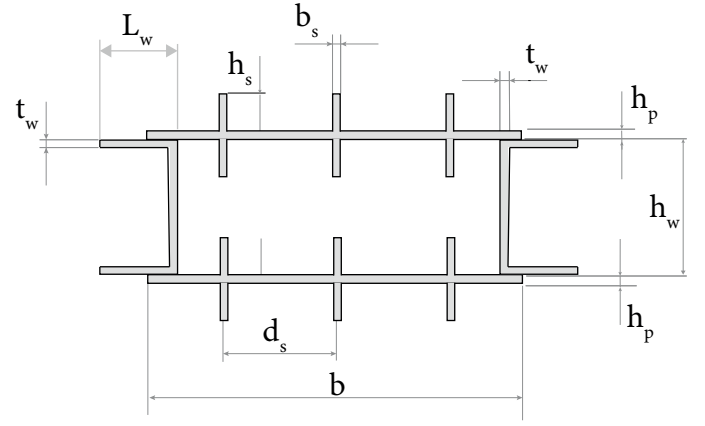

Fig. 1 : Example of the box-beam cross section considered in this work.

2 Mathematical model

The derivation of the governing equations of the unitized beam starts with the derivation of the equivalent continuum plate stiffnesses of the stiffened panels. The latter are used to derive the equivalent beam model by means of the Circumferentially Asymmetric Stiffness (CAS) model. For the interest of clarity, an example of the box beam's cross section is depicted in Fig. 1 where all the relevant dimensions are indicated.

2.1 Derivation of the equivalent plate properties of unitized panel

The structural model is derived on the basis of the Reissner-Mindlin plate theory. Consistently, the stiffeners are modeled using the Timoshenko beam theory. The kinematic equivalence is enforced within a small repetitive element henceforth referred to as sub-cell. The strain energy density equivalence is applied to the repetitive cell, i.e. to the area enclosed between two adjacent stiffeners. In the interest of clarity, Fig. 2 shows and example of of the repetitive sub-cell and cell, respectively.

The local orientation of the stiffeners is presumed to vary linearly as in Wu et al [17] for tow-placed fibers and Wang et al [18, 19] for curved stiffeners. The stiffeners' orientation $\vartheta(x)$
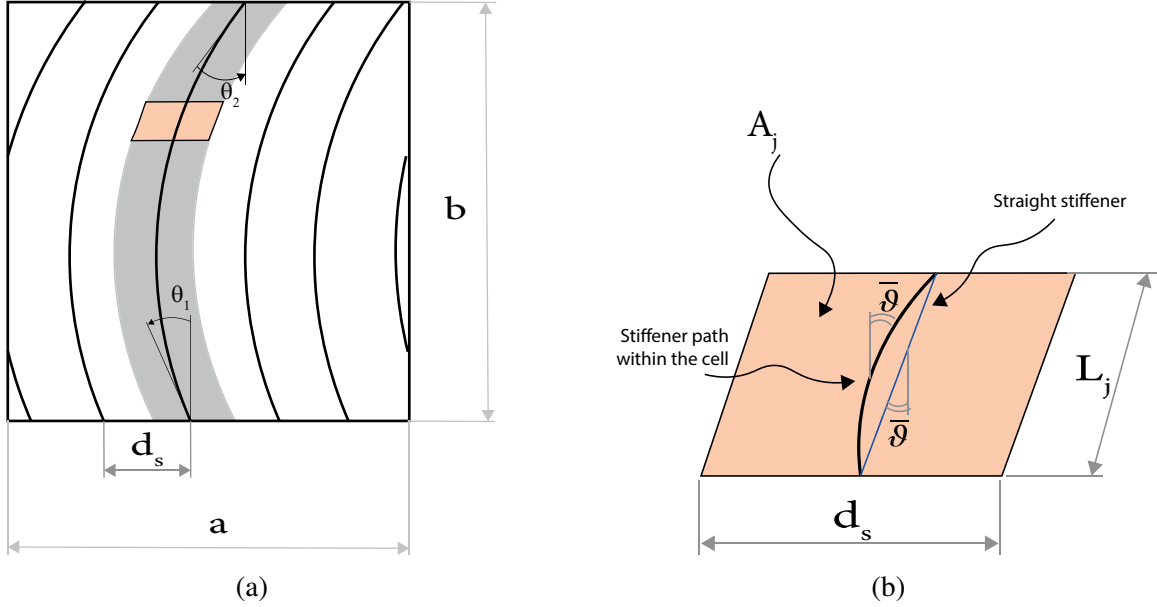
Fig. 2 : Example of the basic cell Figure (a) (shaded gray area) and sub-cell (b) (shaded red area).

is given as

$$\vartheta(x) = \vartheta_1 + \frac{\vartheta_2 - \vartheta_1}{b}x, \qquad (1)$$

being b the panel length, as shown in Figure 2. The stiffeners are presumed being oriented at an angle $\vartheta(x)$ with respect to the x-axis of the plate. The prismatic rectangular stiffeners are in the symmetric (or concentric) configuration and perfectly bonded to the skin panel. The kinematic equivalence is established imposing that the strains in any point of the equivalent continuum layer are equal to the strains in any point of the stiffeners. The variation of the strain along the stiffeners width is neglected, consistently with the plate's theory assumption that $M_z = 0$. Moreover, since the shear and twisting deformations act only on one face of the stiffeners while on both faces of the differential plate element, the stiffeners are presumed contributing only to half of the shear deformation.

In matrix form, the strains of the beam element rewritten using the usual notation for plate theory (see Reddy [22]) are given as

$$\{\varepsilon_b\} = [E]\{\varepsilon_P\}. \qquad (2)$$

Equation 2 relates the generalized strains of the Timoshenko beam model to those of the Reissner-Mindlin plate model. The strain energy for the Timoshenko beam can be written as in Nemeth [23]. Being $[C_b]$ the constitutive matrix for the beam and denoting with L_j the length of the sub-cell, the strain energy for the beam is given as

$$U_b = \frac{1}{2} \int_{L_j} \{\varepsilon_b\}^T [C_b]\{\varepsilon_b\} \mathrm{d}X \qquad (3)$$

Equivalently, recalling that $\varepsilon_P^T = \{\varepsilon_{xx}^{(0)}, \varepsilon_{yy}^{(0)}, \gamma_{xy}^{(0)}, \kappa_{xx}^{(0)}, \kappa_{yy}^{(0)}, \kappa_{xy}^{(0)}, \gamma_{yz}^{(0)}, \gamma_{xz}^{(0)}\}$, the strain energy for the beam written in the equivalent plate-strains assumes the following form

$$U_P = \frac{1}{2} \int_{L_j} \{\varepsilon_P\}^T [C_P]\{\varepsilon_P\} \mathrm{d}X, \qquad (4)$$

where $[C_P] \in \mathbb{R}^{8 \times 8}$ is given as

$$[C_p] = [E]^T [C_b][E]. \qquad (5)$$

Equation 5 is written in the beam (stiffener) reference frame and must be rotated to align the beam reference system XYZ to the global reference system xyz (plate system). It follows that

$$U_p = \frac{1}{2} \int_{L_j} \{\varepsilon_p\}^T [C_p]\{\varepsilon_p\} \mathrm{d}x, \qquad (6)$$

$$\text{where} \qquad [C_p] = [T]^T [C_P][T].$$

The transformation $T \in \mathbb{R}^{8,8}$ matrix is given as

$$
\begin{bmatrix}
[T_\varepsilon] & [0] & [0] \\
[0] & [T_\varepsilon] & [0] \\
[0] & [0] & [T_t]
\end{bmatrix}, \tag{7}
$$

Based on the assumption that the sub-cell is sufficiently small, the strain energy can be approximated as follow

$$
U_p = \frac{L_j}{2} \{\varepsilon_p\}^T [C_p] \{\varepsilon_p\}, \tag{8}
$$

the strain energy density per unit area is given by

$$
\hat{U}_p = \frac{U}{A_j} \tag{9}
$$

where A_j is the area of the sub-cell. From Figure 2 follows that $A_j \approx L_j d_s \cos \hat{\vartheta}$. The strain energy density for the equivalent continuum layer is given as

$$
2\hat{U} = n_s \sum_{j=1}^{n_{sc}} \frac{\{\varepsilon_p\}^T [C_p] \{\varepsilon_p\}}{d_s \cos \hat{\vartheta}} = \int_0^{h_s} \{\varepsilon\}^T [Q] \{\varepsilon\} \mathrm{d}z, \tag{10}
$$

where n_s is the number of stiffeners, n_{sc} is the number of sub-cells, and $[Q]$ on the right-hand side of the Eq. 10 is the reduced stiffness matrix of the equivalent-continuum layer, consistent with the derivation presented in [24]. Likewise, in the limit for $n_{cell} \to \infty$ one notes the following

$$
\lim_{n_{cell} \to \infty} \bar{\vartheta} \to \vartheta(x),
$$

$$
\lim_{n_{cell} \to \infty} 2\hat{U} \Rightarrow \int_0^{h_s} \{\varepsilon\}^T [Q(x)] \{\varepsilon\} \mathrm{d}z. \tag{11}
$$

Finally, taking the derivatives of the quadratic forms given in the Equations 10 and 11 respectively, yields the stiffness matrices of the equivalent continuum layer. It is worth noticing that the equivalent properties obtained using Eq. 11 are those of a variable stiffness layer, in the following denoted as $EqVS$ while, Eq. 10, give rise to an equivalent constant stiffness model, denoted as EqH.

In order to assess the validity of the equivalent continuum model derived herein are two examples with different topologies of the stiffeners. Specifically, the buckling loads and natural

Table 1: Geometric features of the stiffened panels under study.

Young's modulus	E	73 GPa
Poisson ratio	ν	0.3
Density	ρ	2780 kg/m^3
Stiffeners' width	b_s	3 mm
Stiffeners' spacing	d_s	100 mm
Stiffeners' height	h_s	20 mm
Number of stiffeners	n_s	5
Plate's skin thickness	h_p	3 mm
Panel's width	a	500 mm
Panel's length	b	800 mm

frequencies of rectangular panels are considered. The panels are simply supported along the edges and, for the case of buckling loads, are subjected to uni-axial compression N_x. The results obtained with the equivalent models are compared against those obtained modeling the skin plate and the stiffeners with shell elements (QUAD4), as depicted in Fig. 3. The results pertaining the two cases analyzed are reported in Tab. 2 and Tab. 3. A good agreement is found among the equivalent model and the detailed model. It can be noted from Tables 2 and 3 that the $EqVS$ model is more accurate than the EqH in either cases. On the basis of the results reported herein, it can be stated that the stiffness variability introduced by the curved stiffeners cannot be neglected. A more extensive analysis and discussion, along with several other examples, can be found in the first author's PhD dissertation [25].

2.2 Unitized box-beam model

In the following analysis only the flap-torsion coupling is retained. This assumption derives from the particular arrangement of the panels chosen in this work, i.e. concentric panels with same topology of the stiffeners for the upper and lower panels. Moreover, the aft and fore panels are unstiffened C-beams.
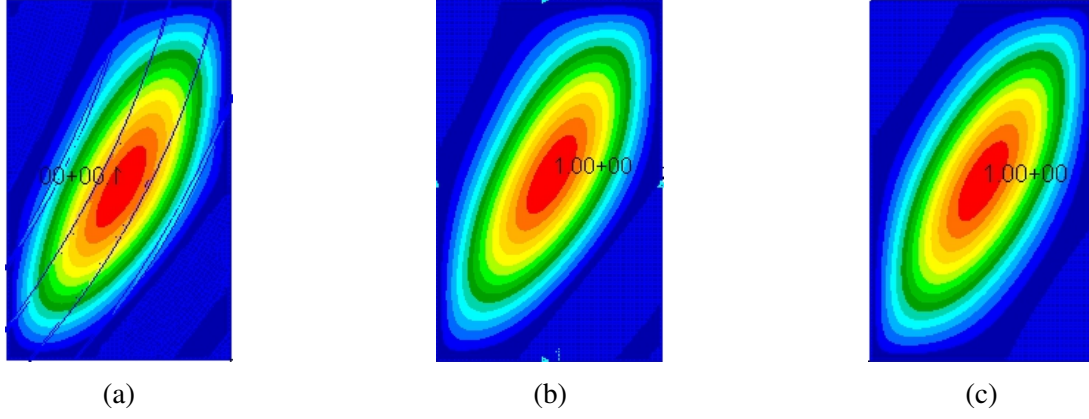
The circumferentially asymmetric stiffness

(a) (b) (c)

Fig. 3 : Comparison of the buckling modes of a stiffened panel with $\vartheta_1 = -40°$ and $\vartheta_2 = -14°$. Fig. (a) is the first buckling mode of the stiffened structure, while Fig. (b) and Fig. (c) are the first buckling mode for the case of variable ($EqVS$) and constant (EqH) stiffness respectively.

Table 2: First buckling load [N/mm] of simply supported panels with curved stiffeners subjected to uni-axial compression N_x.

	Topology θ_1	θ_2	Stiffened	Eq. V.S.	$Err_{R\%}$	Eq. H.	$Err_{R\%}$
a	$-40°$	$-14°$	293.2	300.0	2.3	338.19	15.3
b	$10°$	$34°$	292.7	293.2	0.2	313.5	7.1

Table 3: First frequencies [Hz] of a simply supported panels with curved stiffeners.

	Topology θ_1	θ_2	Stiffened	Eq. V.S.	$Err_{R\%}$	Eq. H.	$Err_{R\%}$
a	$-40°$	$-14°$	114.25	115.01	0.7	118.65	3.8
b	$10°$	$34°$	103.91	108.78	-4.7	112.46	7.6

coefficients are given as follows

$$GJ = \frac{4\Omega^2}{\oint 1/A^*_{66}ds} + 4\oint D^*_{66}ds \quad (12a)$$

$$k = 2\Omega\frac{\oint \left(A^*_{16}/A^*_{66}\right) z ds}{\oint 1/A^*_{66}} ds - 2\oint D^*_{16}\left(\frac{dy}{ds}\right)ds \quad (12b)$$

$$EI_2 = \oint z^2\left(A^*_{11} - \frac{A^{*2}_{16}}{A^*_{66}}\right)ds + \frac{\left[\oint A^*_{16}/A^*_{66}zds\right]^2}{\oint 1/A^*_{66}ds}$$
$$+ \oint D^*_{11}\left(\frac{dy}{ds}\right)^2 ds \quad (12c)$$

$$EI_3 = \oint y^2\left(A^*_{11} - \frac{A^{*2}_{16}}{A^*_{66}}\right)ds + \frac{\left[\oint A^*_{16}/A^*_{66}yds\right]^2}{\oint 1/A^*_{66}ds}$$
$$+ \oint D^*_{11}\left(\frac{dz}{ds}\right)^2 ds \quad (12d)$$

Retaining only the membrane contributions to the stiffnesses, the above equations agree with those given in [26, 27], while, the expression as reported in Eqns 12 are in agreement with [20] where also the bending contributions to the stiffness were considered. It is worth mentioning that, despite the integral reported in the Eqns 12, they are limited to the area enclosed by the midline of the thin walled beam, also the contribu-

5

tions of the spar's flanges has been considered to compute the overall beam stiffness.

In Figure 4 are reported the effective beam properties GJ_t, k, EI_2 with respect to the angles of orientation of the stiffeners ϑ_1, ϑ_2. For the sake of simplicity we neglected the variation of the stiffness coefficients with respect to the beam abscissa that is, the expression of the effective beam properties are calculated using the homogenized coefficients (see Eq. 10). It is seen that the maximum coupling k can be obtained with straight stiffeners oriented at $\vartheta = 27.5°$. It is worth noting that the maximum bending stiffness is given for stiffeners oriented at zero while, orienting the stiffeners at $\vartheta = 45°$ ensures the maximum torsional stiffness GJ_t. Figure 5 illustrates the variation of the effective beam stiffnesses with respect to the beam abscissa x when the upper and lower panels have curved stiffeners with $\vartheta_1 = 0, \vartheta_2 = 25$; all the others geometric parameters for the unitized beam are listed in Table 4. The solid lines are the variable stiffness properties while the dashed lines are for the homogenized beam stiffnesses. Figure 6 shows the attainable effective beam stiffnesses when ϑ_2 varies within the entire range of possible orientations while ϑ_1 is changed parametrically[1].

The governing equations for the flexural-flexural-torsional, variable stiffness beam are given as follow .

$$-(GJ)'\varphi' - GJ\varphi'' + k'w'' + kw''' = q_\varphi, \qquad (13a)$$

$$-k''\varphi' - 2k'\varphi'' - k\varphi''' + (EI_2)'' w'' + \\ 2(EI_2)' w''' + EI_2 w^{IV} = q_w, \qquad (13b)$$

$$(EI_3)'' v'' + 2(EI_3)' v''' + EI_3 v^{IV} = q_v. \qquad (13c)$$

Note that the case of constant stiffness can be recovered from Eqns 13 neglecting the derivatives of the stiffness' coefficients; moreover, the case of isotropic structure can be obtained by assuming the coupling term k equals zero.

---

[1] The curves reported in Figure 6 are the contour plots of the envelopes shown in Figure 4

3 Problem formulation

The topology optimization problem is formulated such that the design variables are the stiffeners' orientations at prescribed control points. All the other geometric parameters are fixed (see Table 4). The optimization problem for the static cases can be formulated as follows

$$\textbf{max} \quad \frac{1}{2}\int_0^L \left(\frac{M_y^2 GJ_t}{GJ_t EI_2 - k^2} \right) dx \qquad (14)$$

$$\text{subject to:} \quad \mathbf{Ku} = \mathbf{q}$$

$$\vartheta_1^{i+1} = \vartheta_2^i$$

$$-45° \leq \vartheta_i \leq 45°$$

$$\varphi_{tip} \geq \varphi_0$$

$$w_{tip} \leq w_0$$

where $\mathbf{u}$ is the vector of the generalized displacement $\mathbf{u} = [\rho_x \ \rho_y \ \rho_z]^T$, $\mathbf{K}$ is the stiffness matrix, ϑ_i is the angle of orientation of the stiffeners at control point i, and $\mathbf{q} = [M_t \ M_{flap} \ M_{lag}]^T$ is the generalized force vector. The stiffness matrix is given as follow

$$\mathbf{K} = \begin{bmatrix} GJ_t & K & 0 \\ k & EI_2 & 0 \\ 0 & 0 & EI_3 \end{bmatrix}$$

In the case of planar deformation (i.e. $\rho_z = 0$), the strain energy (compliance) is given as follow

$$\frac{1}{2}\int_0^L \left(\frac{M_y^2 GJ_t}{GJ_t EI_2 - k^2} \right) dx. \qquad (15)$$

The optimization is carried out by means of the Stud^p GA, i.e. a population based algorithm which implement the breeding farm paradigm to enhance the algorithm exploration and exploitation. A stress parameter η of 0.4 and a probability of extinction of 0.8 have been selected; the reader can refer to Danzi *et al* [28, 29] for further details. A population of 20 chromosomes is used. Standard mutations has been implemented; the cross over probability is set to 1. The allowable orientations range from $\vartheta = -45°$ to $\vartheta = 45°$ with a set space of 2.5°.
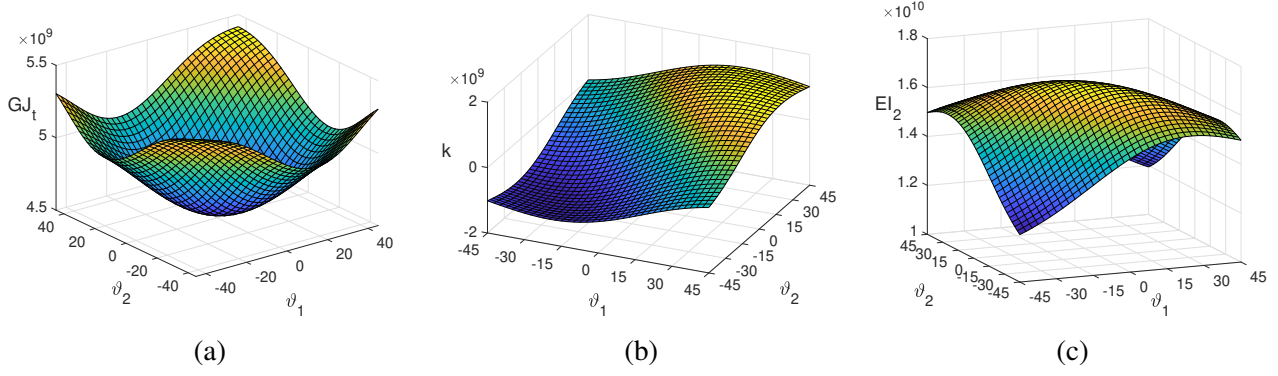
(a)　　　　　　　　　　　(b)　　　　　　　　　　　(c)

Fig. 4 : Effective beam properties with respect to the stiffeners' orientations ϑ_1, ϑ_2. The envelopes are obtained considering the homogenized properties.

4 Results

The wing box under study is made by Al 6060 Aluminum alloy ($E = 58000$ MPa, $v = 0.33$ and $\rho = 2780$ kg/m^3). With reference to Fig. 1, all the other geometrical parameters, i.e. aft and fore panels thicknesses t_w, plate's skin thickness h_p, stiffeners width b_s and height h_s, cross sectional width b and height of the shear webs h_w are fixed. For the sake of clarity, the corresponding values are listed in Table 4 . Three static cases are considered, namely: (a) tip concentrated load, (b) uniform distributed load and (c) triangular load. For all the cases considered, only q_w is applied. The load is applied at the cross-sectional centroid. The following pairs of tip displacements w_0 and rotations φ_0 are given for the three problems in hand, namely: concentrated load $\{14$ mm, $0.287°\}$, uniformly distributed load $\{4.6$ mm, $0.08°\}$ and triangular load $\{1.1$ mm, $0.03°\}$.

The first load case is the same used in Cestino [20, 21] considered herein as benchmark to validate the mathematical model derived. The beam is clamped at one end and subjected to a concentrated load $F = 41.37$ kg applied with an offset of 40 mm with respect to the beam tip. Two transducers are placed at the beam's tip in order to measure the deflection and rotation respectively, as shown in Figure 7. In Figure 8 is reported the comparison between the stiffnesses predicted with the present model and those obtained as in [20]. A small deviation with respect
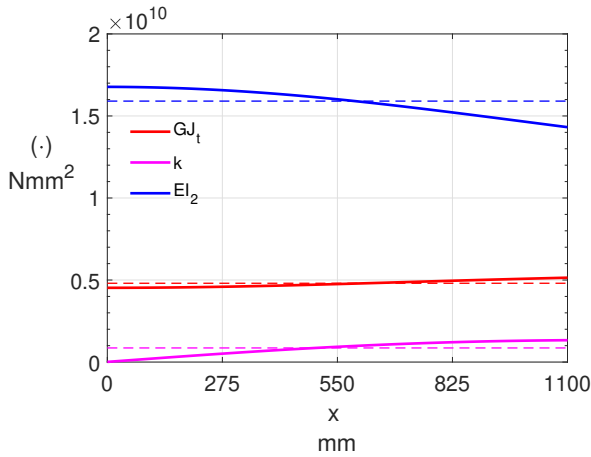

Fig. 5 : Effective beam stiffnesses with respect to the beam abscissa x for the case of curvilinear stiffeners $\vartheta_1 = 0°, \vartheta_2 = 25°$. Solid lines represent the variable stiffnesses while the dashed lines are the homogenized stiffnesses.
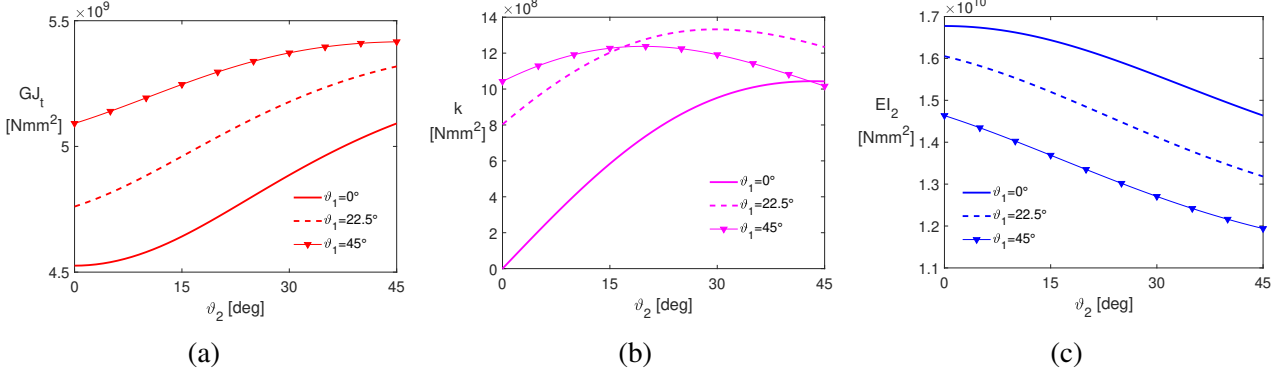
(a) (b) (c)

Fig. 6 : Effective beam properties with respect to the stiffeners' orientation ϑ_2 at fixed ϑ_1. Solid lines are for $\vartheta_1 = 0°$, dashed lines are for $\vartheta_1 = 22.5°$ and the marker are for $\vartheta_1 = 45°$. The envelopes are obtained considering the homogenized properties.

Table 4: Geometric features of the wing box under study.

Stiffeners' width	b_s	3 mm
Stiffeners' spacing	d_s	10 mm
Stiffeners' height	h_s	4 mm
Number of stiffeners	n_s	6
Plate's skin thickness	h_p	2 mm
Beam's length	L	1100 mm
Spar caps length	L_w	20 mm
Spar height	h_w	40 mm
Spar's thickness	t_w	2 mm

to the stiffnesses computed as in [20] is appreciable; the deviation is due to the model adopted to calculate the bending stiffnesses. Indeed, Cestino and Frulla considered the bending stiffness of the stiffened plate being calculated as for solid panels, that is $[D] = [Q](h_+^3 - h_-^3)$. Danzi [25] noted that this lead to a discrepancy with respect to the stiffnesses attainable using Nemeth's formulation [23], especially for thicker stiffeners. In this case, however, the stiffeners' height is comparable with that of the skin plate therefore the aforementioned discrepancy is small. Figure 9 reports the bending displacement and the rotation of the beam measured at the beam's tip. Different models, namely: (a) solid FE mode, (b) theoretical derivation as in Cestino [20], (c) experiment and (d) present derivation for the case of

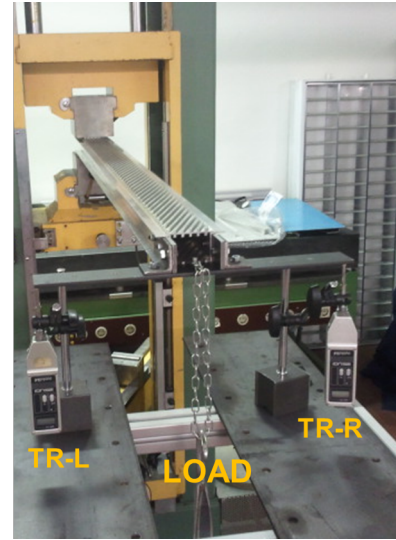straight stiffeners oriented at $25°$ are compared against each other.

Fig. 7 : Experimental setup for the first load case with straight stiffeners oriented at $25°$.

The beam tip deflection and rotation for the different load cases are listed in Table 5. The last column of Table 5 exemplifies the optimized topology for the stiffeners path. It is worth noting that, differently to Cestino [20], the optimum orientation of the stiffeners for the case of concentrated load is at $27.5°$ rather than $27.5°$. The results are in agreement with those obtained in [21] where a topology optimization was performed using the SIMP algorithm. Examining the case of uniformly distributed
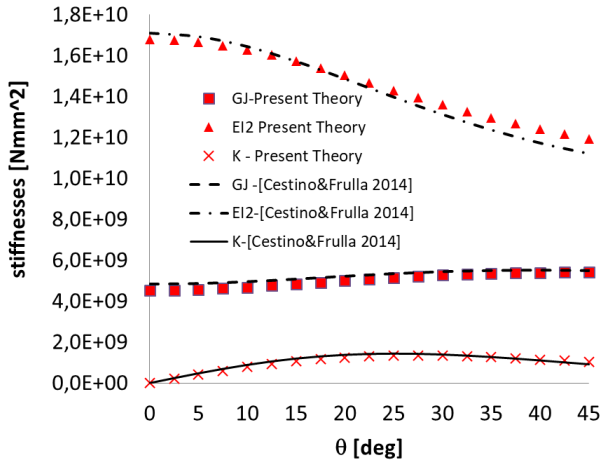
Fig. 8 : Comparison of the stiffnesses obtained with the presented model and the model adopted in [20].
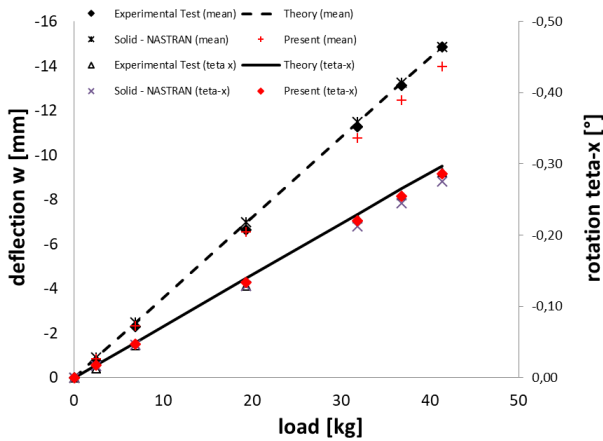

Fig. 9 : Comparison of the mean tip displacement and tip rotation obtained with different models and experiments.

load, the optimization leads to curved stiffeners with $\vartheta_1 = 20°$ and $\vartheta_2 = 22.5°$. It is seen that the problem is multi-modal, particularly, since the homogenized model have been considered herein, the solution $\vartheta_1 = 20°$ and $\vartheta_2 = 22.5°$ is equivalent to the solution $\vartheta_1 = 22.5°$ and $\vartheta_2 = 20°$. The same behavior has been observed for the case of triangular distributed load, in this case the optimum orientations are $\vartheta_1 = 5°$ and $\vartheta_2 = 12.5°$.
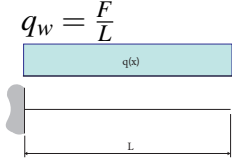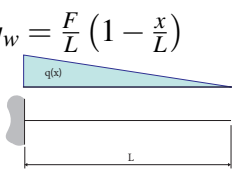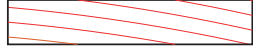
5   Conclusions

In this work, a Strain-Energy-based equivalence method has been adopted to derive the equivalent continuum model of curvilinear stiffened plates. It is shown that the derivation gives rise to two equivalent plate models, i.e. equivalent constant stiffness and equivalent variable stiffness. The two models have been assessed comparing buckling loads and frequencies of vibrations of simply supported, rectangular plate. The comparison were made by means of FEA with respect to the buckling loads and frequencies obtained considering the stiffened structure. It is shown that the variable stiffness model gives better accuracy with respect to the constant model and thus should be preferred to the constant stiffness one.

A unitized box-beam made by an arrangement of stiffened and unstiffened panels has been then considered. By means of CAS model, the effective beam cross-sectional properties have been calculated. A parametric analysis has been performed in order to investigate the effect of the stiffeners orientations on to the apparent beam stiffnesses. A comparison of the effective beam stiffnesses with variable and constant stiffnesses is presented for one case aiming to highlight the differences between the two models. It has been observed that for the cases analyzed herein the difference between the stiffnesses attainable with the two models is small.

The effect of the applied load to the stiffeners' path is investigated. Particularly solutions which maximize the compliance (strain energy) given a set of requirements in term of maxi-

Table 5: Results of the topology optimization for the static cases.

Load	$\vartheta_i[deg]$	$w[mm]$	$\varphi[deg]$	Topology[1]
$q_w = \delta(L)F$	$\vartheta_1 = 27.5$ $\vartheta_2 = 27.5$	-13.89	-0.29	
$q_w = \frac{F}{L}$	$\vartheta_1 = 20$ $\vartheta_2 = 22.5$	-4.548	-0.801	
$q_w = \frac{F}{L}\left(1 - \frac{x}{L}\right)$	$\vartheta_1 = 5$ $\vartheta_2 = 12.5$	-1.0994	-0.0317	

[1] The beams are drawn out of scale.

mum tip deflection and minimum tip rotation are sought. The optimization has been performed using the Stud[p] GA. The optimization problem has been written as topology optimization where the design variables were the orientations of the stiffeners at the root and tip of the beam respectively. A good agreement between numerical and experimental results is found. The results obtained are in agreement with results in published literature.

In conclusion, the authors envision that the low fidelity model presented here will be useful in the preliminary design stages of an aircraft. Indeed, it has been shown that despite using a limited set of degrees of freedom and a minimum number of design variables, the model and subsequent analysis can qualitatively predict the behavior of complex structures. It is useful in obtaining insights for the successive design stages. Moreover, it offers the advantage of being computationally efficient, the opposite of cumbersome Finite-Element-based optimization using commercial software.

References

[1] Cestino E, Frulla G, Perotto E and Marzocca P. Experimental Slender Wing Model Design by the Application of Aeroelastic Scaling Laws. *Journal of Aerospace Engineering*, DOI:10.1061/(ASCE)AS.1943-5525.0000211, pp.112-120, ISSN:0893-1321, vol. 27 (1), 2014.

[2] Cestino E, Frulla G, Perotto E and Marzocca P. Theoretical and Experimental Flutter Predictions in High Aspect Ratio Composite Wings, *SAE INTERNATIONAL JOURNAL OF AEROSPACE*, pp. 1365-1372, ISSN: 1946-3855, 2011

[3] Frulla G, Cestino E and Marzocca P. Critical Behaviour of Slender Wing Configurations. *Journal of Aerospace Engineering - Part G*, DOI:10.1243/09544100JAERO553, ISSN:0954-4100, pp.587-600, vol. 224, 2010.

[4] Jutte C V and Stanford, B K. Aeroelastic Tailoring of Transport Aircraft Wings: State-of-the-Art and Potential Enabling Technologies,*NASA TM-2014-218252*, Langley Research Center, Hampton, Virginia, 2014.

[5] Munk M. Propeller Containing Diagonally

Disposed Fibrous Material, *U.S. Patent US77046047A*, Oct. 1949.

[6] Weisshaar T. Aeroelastic Tailoring - Creative Uses of Unusual Materials,*28th Structures, Structural Dynamics and Materials Conference, Structures, Structural Dynamics, and Materials and Co-located Conferences*, 1987.

[7] Weisshaar T, Nam C and Batista-Rodriguez A. Aeroelastic Tailoring for Improved UAV Performance. *AIAA Structures, Structural Dynamics, and Materials Conference*, Long Beach, CA, April 20-23, 1998.

[8] Haftka R. Parametric Constraints with Application to Optimization for Flutter Using a Continuous Flutter Constraint,*AIAA Journal*, Vol. 13, pp. 471-475, 1975.

[9] Stroud W, Krishnamurthy T, Mason B, Smith S and Naser A. Probabilistic Design of a Plate-Like Wing to Meet Flutter and Strength Requirements. *AIAA Structures, Structural Dynamics, and Materials Conference*, Denver, CO, April 22-25, 2002.

[10] Martins J, Alonso J and Reuther J. High-Fidelity Aero-Structural Design Optimization of a Supersonic Business Jet. *AIAA Structures, Structural Dynamics and Materials Conference*, Denver, CO, April 22-25, 2002.

[11] Maute K and Allen M. Conceptual Design of Aeroelastic Structures by Topology Optimization. *Structural and Multidisciplinary Optimization*, Vol. 27, pp. 27-42, 2004.

[12] Pettit C and Grandhi R. Optimization of a Wing Structure for Gust Response and Aileron Effectiveness, *Journal of Aircraft*, Vol. 40, No. 6, pp. 1185-1191, 2003.

[13] Cooper A. Trajectorial Fiber Reinforcement of Composite Structures, *Ph. D. Dissertation*, Washington University, St. Louis, Missouri, 1972.

[14] Kapania R K, Li J and Kapoor H, Optimal Design of Unitized Panels with Curvilinear Stiffeners, *AIAA 5th Aviation, Technology, Integration, and Operations Conference*, Arlington, Virginia, 26 - 28 Sep 2005.

[15] Larson W J and Pranke L K. *Human Spaceflight: Mission Analysis and Design*, McGraw-Hill, ISBN 978-0077230289,1999.

[16] Roskam J. *Airplane Desing*. DARcorporation,

ISBN 188488542X, 9781884885426,1985.

[17] Wu C, Gurdal Z and Starnes J. Structural Response of Compression-Loaded, Tow-Placed, Variable Stiffness Panels, *Proc 43rd AIAA/ASME/ASCE/AHS/ASC Structures, Structural Dynamics, and Materials Conference, Structures, Structural Dynamics, and Materials and Co-located Conferences*, Denver (CO), United States, 22-24 April 2002.

[18] Wang D and Abdalla M M, Global and local buckling analysis of grid-stiffened composite panels, *Composite Structures*. Vol 119, pages 767 - 776, 2015.

[19] Wang D and Abdalla M M, Buckling optimization of steering stiffeners for grid-stiffened composite structures, *20th International Conference on Composite Materials*, Copenhagen, 19-24 July 2015.

[20] Cestino E and Frulla G. Analysis of slender thin-walled anisotropic box-beams including local stiffness and coupling effects. *Aircraft Engineering and Aerospace Technology: An International Journal*, Vol. 86 Issue 4 pp. 345 -355, 2014.

[21] Cestino E, Frulla G, Duella R, Piana P, Pennella F and Danzi F. Application of Structural Topology Optimization to Couple Thin-Walled Stiffened Box-Beams. *Proc SAE 2017 AeroTech Congress& Exhibition*, DOI:10.4271/2017-01-2059, ISSN:0148-7191, September 26-28, Fort Worth (TX), United States, 2017.

[22] Reddy J N. *Mechanics of Laminated Composite Plates and Shells: Theory and Analysis*. Taylor & Francis, ISBN 0849315921, 97808493159232004.

[23] Nemeth M P. A Treatise on Equivalent-plate Stiffnesses for Stiffened Laminated-composite Plates and Plate-like Lattices. *NASA technical paper*. National Aeronautics and Space Administration, Langley Research Center, Virginia, USA, 2011.

[24] Danzi F, Cestino E, Frulla G and Gibert J M. Equivalent Plate Model Of Curvilinear Stiffened Panels. *Proc 7th International Conference on Mechanics and Materials in Design*, Albufeira,Portugal, 11-15 June 2017.

[25] Danzi F. Dynamic Tailoring of beam-like structures.*PhD Thesis*. Politecnico di Torino, Italy,

2018.

[26] Frulla G and Cestino E. Flutter analysis of a high aspect ratio composite wing test-model. *Proc. AIRTEC 5th International ConferenceâĂŞSupply on the Wings*. Frankfurt, Germany, 2-4 November 2010.

[27] Frulla G and Cestino E. Structural analysis of slender composite thin-walled box-beam for aeroelastic applications. *Proc. AIRTEC 6th International ConferenceâĂŞSupply on the Wings*. Frankfurt, Germany, 2-4 November 2011.

[28] Danzi F, Frulla G and Cestino E. Constrained combinatorial optimization of multi-layered composite structures by means of Stud GA with proportionate selection and extinction.*Structural And Multidisciplinary Optimization*, DOI:10.1007/s00158-016-1638-4, pp.2239-2257, ISSN:1615-1488, vol. 55 (6), 2017.

[29] Danzi F, Frulla G, Cestino E and Gibert J M. MDO/MSO of Slender Thin Walled Box Beam Model. *Proc AIAA/ISSMO Multidisciplinary Analysis and Optimization Conference*, DOI:10.2514/6.2017-4323, ISBN:978-1-62410-507-4, Denver (CO), United States, June 5-9, 2017.

6 Contact Author Email Address

The corresponding author can be contacted at the following email addresses: francesco.danzi@polito.it or fdanzi@purdue.edu

Copyright Statement